Structure of the floating water bridge and water in an electric field

Lawrie B. Skinner[a,b,c,1], Chris J. Benmore[a], Badri Shyam[a], J. K. R. Weber[a,c], and John B. Parise[b,d]

[a]X-ray Science Division, Advanced Photon Source, Argonne National Laboratory, Argonne, IL 60439; [b]Mineral Physics Institute and Department of Geosciences, Stony Brook University, Stony Brook, NY 11794-2100; [c]Materials Development Inc., Evanston, IL 60202; and [d]Photon Science Division, Brookhaven National Laboratory, Brookhaven, NY 11973

Edited by Richard J. Saykally, University of California, Berkeley, CA, and approved September 5, 2012 (received for review July 5, 2012)

The floating water bridge phenomenon is a freestanding rope-shaped connection of pure liquid water, formed under the influence of a high potential difference (approximately 15 kV). Several recent spectroscopic, optical, and neutron scattering studies have suggested that the origin of the bridge is associated with the formation of anisotropic chains of water molecules in the liquid. In this work, high energy X-ray diffraction experiments have been performed on a series of floating water bridges as a function of applied voltage, bridge length, and position within the bridge. The two-dimensional X-ray scattering data showed no direction-dependence, indicating that the bulk water molecules do not exhibit any significant preferred orientation along the electric field. The only structural changes observed were those due to heating, and these effects were found to be the same as for bulk water. These X-ray scattering measurements are supported by molecular dynamics (MD) simulations which were performed under electric fields of 10^6 V/m and 10^9 V/m. Directional structure factor calculations were made from these simulations parallel and perpendicular to the E-field. The 10^6 V/m model showed no significant directional-dependence (anisotropy) in the structure factors. The 10^9 V/m model however, contained molecules aligned by the E-field, and had significant structural anisotropy.

water electric field | pair distribution function | temperature dependence | high voltage

It is well known that a stream of water can be deviated by the static electricity on a plastic rod (1) and this has often been explained by the water molecules being "partially aligned in the electric field" (2). The arrangement of water molecules in electric fields and at charged surfaces has important implications in electrochemistry, mineralogy, and biology (3–5). Hydrogen bonding is weakened perpendicular to very high electric fields (approximately 10^9 V/m), and strengthened along the direction of the field. This modification of the hydrogen bonding is due to partial alignment of the water molecules, and affects the existing three-dimensional network in an anisotropic manner. In weaker electric fields a striking visual illustration of the effect of high voltage applied to pure water is the formation of a stable thread, a few millimeters in diameter between two beakers, known as the floating water bridge (6). Under these conditions, electric fields of approximately 10^6 V/m enable the free standing bridge to facilitate water flow from one beaker to another over a distance of up to approximately 25 mm (the field strength estimate is calculated from the applied voltage divided by the bridge length). This water bridge phenomenon is essentially an extension of the Taylor cone, and cone-jet formations which are responsible for electrosprays. A Taylor cone, first explained in 1964 (7), is the formation of a cone shaped liquid surface due to high electric fields, which at higher field strength deforms further to emit a jet. This cone-jet phenomenon is understood in terms of the surface charge deforming the liquid toward a surface of equal electrical potential.

Recent measurements however, have suggested that there is also preferred orientation of water molecules along the electric field within the floating water bridge (6, 8–14). If correct, this preferred orientation has broader implications for the behavior of water under these relatively modest approximately 10^6 V/m field strengths. Affecting phenomena such as ice formation in supercooled water (15), transport through biological cell membranes (16), (where potential differences are often of comparable magnitude), and electrohydrodynamic behavior, which is typically modeled assuming an unchanged local molecular structure (7).

The key observations in water bridges that motivated this study were: Density gradients (7% edge to core) observed using optical techniques (6), anisotropy observed in neutron scattering (9), optical birefringence from polarized light scattering (11, 12) and changes in the OH stretch vibration from Raman and infrared measurements (10, 13).

Neutron scattering experiments on a floating bridge of D_2O (8) have suggested an increase in scattered intensity at $Q \leq 2$ Å which may be associated with the existence of nano-scale-bubbles (or some other form of nano-scale density fluctuations). Yet a subsequent study by the same group suggests the intensity increase may have been an artifact due to H_2O contamination in the D_2O sample (9). The second neutron study found some anisotropy in the angular distribution of the scattered neutron intensity, although the effect was comparable to the size of the error bars (9). This anisotropy observed in the neutron, and polarized light scattering suggests a preferred orientation of the hydrogen bonded water molecules along the electric field, at a relatively low approximately 10^6 V/m field strength.

Experimentally it is known that water molecules exhibit strong voltage-dependent ordering in fields approximately 10^9 V/m, such as those found within a few molecular layers from the surface of an electrode (3). Similarly density functional theory calculations have shown that electric fields stretch the intermolecular hydrogen bonds in water clusters (17). Above a certain field-strength threshold, these bonds are broken and the water clusters form linear, branched or net-like structures. However, molecular dynamics simulations (18) on small cold water clusters in relatively weak electric fields approximately 10^5 V/m do not show any substantial structural changes. Instead the simulations show an increased molecular vibrational amplitude and molecular reorientation. Other molecular dynamics simulations have suggested that it is the polarization of hydrogen bonds that induces the formation of the water bridge above a threshold field of 1.2×10^9 V/m (19): which is much higher than the approximately 10^6 V/m required to form the bridge experimentally. Alternatively, it has been proposed that ordinary surface tension holds the bridge together rather than the electric field directly (20).

Author contributions: L.B.S., C.J.B., B.S., and J.W. designed research; L.B.S., C.J.B., B.S., J.W., and J.B.P. performed research; L.B.S., J.W., and J.B.P. contributed new reagents/analytic tools; L.B.S. analyzed data; and L.B.S. and C.J.B. wrote the paper.

The authors declare no conflict of interest.

This article is a PNAS Direct Submission.

[1]To whom correspondence should be addressed. E-mail: lawrie.skinner@gmail.com.

This article contains supporting information online at www.pnas.org/lookup/suppl/doi:10.1073/pnas.1210732109/-/DCSupplemental.

PHYSICS

In this work we have performed high-energy X-ray diffraction experiments, with a submillimeter sized beam, on different parts of the floating water bridge (Fig. 1). The main aim of our high-energy X-ray scattering experiment was to measure the bulk intermolecular structure of the floating water bridge, and to look for evidence of structure rearrangement due to the electric field. Particularly any anisotropy (directional dependence) of the scattering pattern, which is indicative of alignment of the water molecules to the electric field. A series of X-ray structure factor measurements were made using different voltages and on different length bridges. High-energy X-ray scattering experiments are well suited to this task as over 90% of the coherent scattering is due to oxygen-oxygen correlations. The low-Q ($0.4 \leq Q \leq 2$ Å^{-1}) signal was also compared to ambient water, to check for nanobubbles or density fluctuations $\lesssim$15 Å ($=2\pi/0.4$) in size. These X-ray diffraction results are compared to molecular dynamic simulated water structure factors calculated in different azimuthal directions, and under different field strengths. This comparison required an extension of the normal liquid structure factor definition to include anisotropy.

The measurements made in this work were performed on beamline 11-ID-C at the Advanced Photon Source using an incident X-ray energy of 114.76(1) keV ($\lambda = 0.10803(1)$ Å). The X-ray intensities were measured using an amorphous-Si area detector as illustrated in Fig. 1. At this energy the X-ray scattering probes the bulk structure of the water, with approximately 96% of the beam being transmitted through the bridge. This high transmission also minimizes background attenuation corrections, which can affect the measured intensity at small angles ($Q \lesssim 2$ Å^{-1}). The background, Compton scattering, self-scattering, and multiple scattering were subtracted using standard methods (21). The corrected X-ray intensity then yields the X-ray weighted structure factor $S^{X}(Q)$. The structure factor is then related to the X-ray weighted differential distribution function $D^{X}(r)$ by sine Fourier transformation. Where $D^{X}(r)$ describes the probability of finding an atom at a separation-r from another atom (for further detail see the *Materials and Methods* section).

Results

Fig. 2 shows three representative X-ray structure factors from a series of water bridges created using different voltages between 8 and 18 kV. For these experiments the bridge lengths varied between 7 mm and 11 mm. The bridge diameters varied between

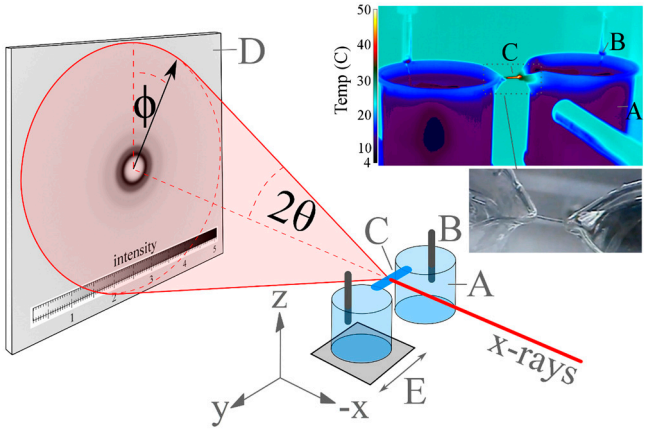

Fig. 1. Setup diagram. A monochromatic high-energy (114.76 keV) X-ray beam is incident on the floating water bridge (*C*) which stretches between two beakers of water (*A*), one of which was moveable (*E*). Platinum electrodes (*B*) are immersed in the beakers with a voltage of approximately 15 kV between them. The 2D scattering pattern is collected by a flat plate area detector (*D*). Top right is an infrared thermal image of the floating water bridge captured when ice water was placed in the two beakers. The lower right image is a photograph of the bridge.

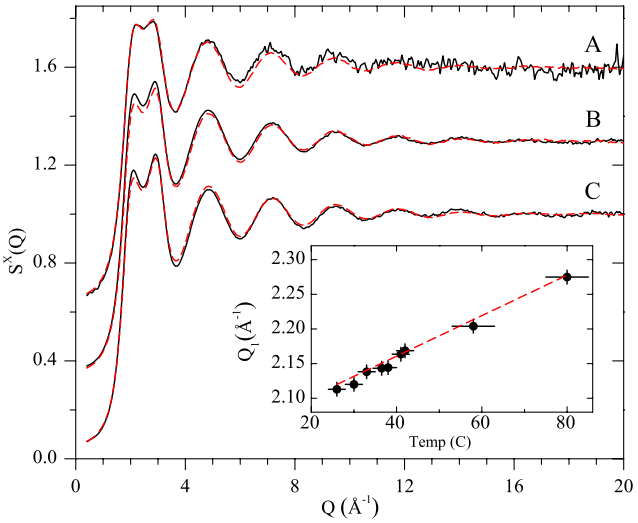

Fig. 2. The black lines are the measured X-ray structure factors for three water bridges. Bridge measurement (*A*) was at 58 °C, using 17 kV, when the bridge was 9.4 mm long. Measurement (*B*) was at 42 °C, using 15 kV, and when the bridge was 7 mm long. Measurement (*C*) was at 26 °C, 15.5 kV, when the bridge was 7 mm long. All three bridges were between 0.8 and 1.3 mm in diameter. The red dashed lines are normal deionized water measured at the same beamline at the corresponding 26 °C, 40 °C, and 60 °C temperatures (see *Materials and Methods* for further detail). The *inset* shows the position of the first maximum in $S^{X}(Q)$, (black circles) against the trend for normal water (red dashed line). Temperature was the only property found to directly correlate with structural change in the water bridge.

0.8 and 1.3 mm. During these experiments the water bridges were generally found to warm up approximately 20 °C over a 30-min period. The X-ray diffraction patterns of the water bridge were measured every 5 min., and were found to correlate strongly with that of bulk water at the same temperature. The position of the first peak in the X-ray structure factor is known to vary linearly with temperature between 20 °C and 80 °C (22), and the floating water bridge data agrees well with the trend observed in bulk water (see Fig. 2, *Inset*).

Fig. 3 shows the X-ray pair distribution functions $D^{X}(r)$, generated from Fourier transforming the $S^{X}(Q)$ patterns shown in Fig. 2. Where the $D(r)$ differential pair distribution functions plotted in Fig. 3 are related to the density normalized pair distribution function $g(r)$, by $D(r) = 4\pi\rho r[g(r) - 1]$, and ρ is the number of molecules per Å^3 (see *Materials and Methods* for further detail). These X-ray weighted $D^{X}(r)$ patterns primarily show intermolecular oxygen-oxygen correlations, and are compared to the $D^{X}(r)$ functions measured for ordinary water at the same temperatures. The observed structural trend with temperature of the water bridge is a reduction in height of the first and second oxygen-oxygen (OO) peaks at 2.8 and 4.5 Å, and an increase in intensity of the region around 3.4 Å, as is seen in bulk water. Ice water was used to affect the temperature of the bridge. However heating of the water within the bridge brought the bridge temperature very close to that observed when room temperature water was used in the beakers (see Fig. 1.). The *inset* in Fig. 3 shows a plot of the first OO peak maximum position in $D^{X}(r)$ as a function of electric field strength for the same nine measurements used in the Fig. 2 *inset*. The difference curve [labeled (D)] in Fig. 3 shows no significant difference in intermolecular structure between the vertical and horizontal ϕ-directions. Whereas the difference curve [labeled (E)] in Fig. 3 shows that there is also no significant difference between ambient water and the water bridge structure measurements.

These results suggest that water retains its bulk network structure along the bridge in the presence of electric fields of approximately 10^6 V/m. The absence of a rise in scattering at the

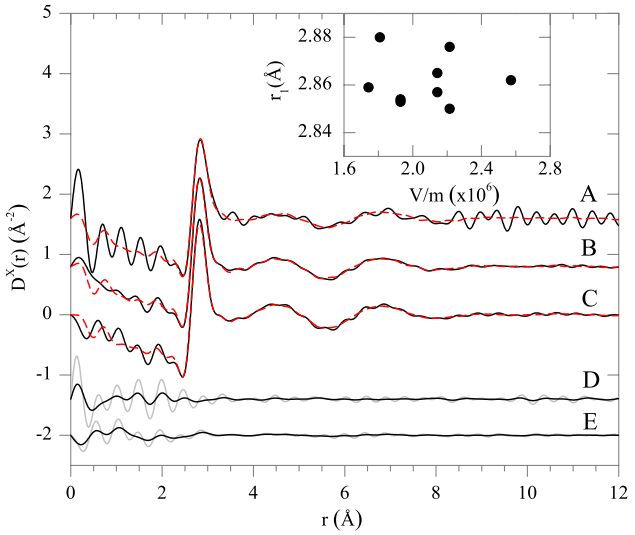

Fig. 3. Shows the $D^X(r) = 4\pi\rho r[g^X(r) - 1]$ differential pair distribution function of the three different temperature water bridge curves in Fig. 2 (labeled *A* to *C*). The black lines are the water bridge measurements, the red dashed lines are the normal water patterns at the corresponding 60 °C (*A*), 40 °C (*B*), and 26 °C (*C*) temperatures. The data was Fourier transformed without using a modification function, and using a maximum Q of 16 Å^{-1}. The lines labeled (*D*) are transforms of the difference between vertical and horizontal slices in $S^X(Q)$, which were both 30 degrees wide. The lines labeled (*E*) are the difference between ambient water at 26 °C and the floating water bridge at 26 °C. In both (*D*) and (*E*) the black lines were transformed using a Lorch modification function (44), whereas the grey lines were transformed without using a modification function. The *inset* shows the position of the oxygen-oxygen peak maximum in $D^X(r)$ against estimated field strength V/m for the same water bridges used in the *inset* in Fig. 2. The error in the measured r_1 position is around 0.01 Å.

minimum-Q measured, compared to that of bulk water, means that we see no evidence of nano-bubbles smaller than ($\approx 2\pi/0.4$) $\approx$15 Å. X-ray diffraction measurements were also performed on different positions horizontally along the length of the bridge, vertically across it, and at a fixed position as a function of applied voltage (between 8–18 kV). The vertical scan in particular probed only the 0.2 mm of water at the top edge of the bridge. All these measurements showed that the water bridge structure was the same as ordinary bulk water at the corresponding temperature.

Plotted in Fig. 4*A* are the structure factors of the water bridge analyzed from 10 degree slices around the azimuthal (ϕ) direction of the X-ray diffraction images. These slices show only a very slight variation in the Q-region 1.5–3.5 Å^{-1}. Further analysis of this Q-region found no consistent ϕ-dependent pattern, and that the slight variation was within the experimental errors. The lack of anisotropy in the 2D X-ray scattering pattern indicates that there is no significant formation of linear chain structures ($\lesssim$1%) in the time-averaged bulk OO structure of the water bridge. This absence of anisotropy is despite observations using Raman spectroscopy (17), and neutron scattering (9), of a slight enhancement of the hydrogen bonding between water molecules within the floating water bridge. This lack of structural anisotropy in the OO distribution is also demonstrated in Fig. 3, which shows the $D^X(r)$ pattern from the difference between the horizontal and vertical directions.

Discussion

Simply viewing the water molecules as dipoles, one would expect that under sufficiently strong electric fields, they would align to that field. This simple picture leads to the idea that the water bridge phenomenon is reinforced by aligned molecules, where the hydrogen bonds are strengthened along the bridge axis. To investigate the sensitivity of our X-ray technique to aligned anisotropic

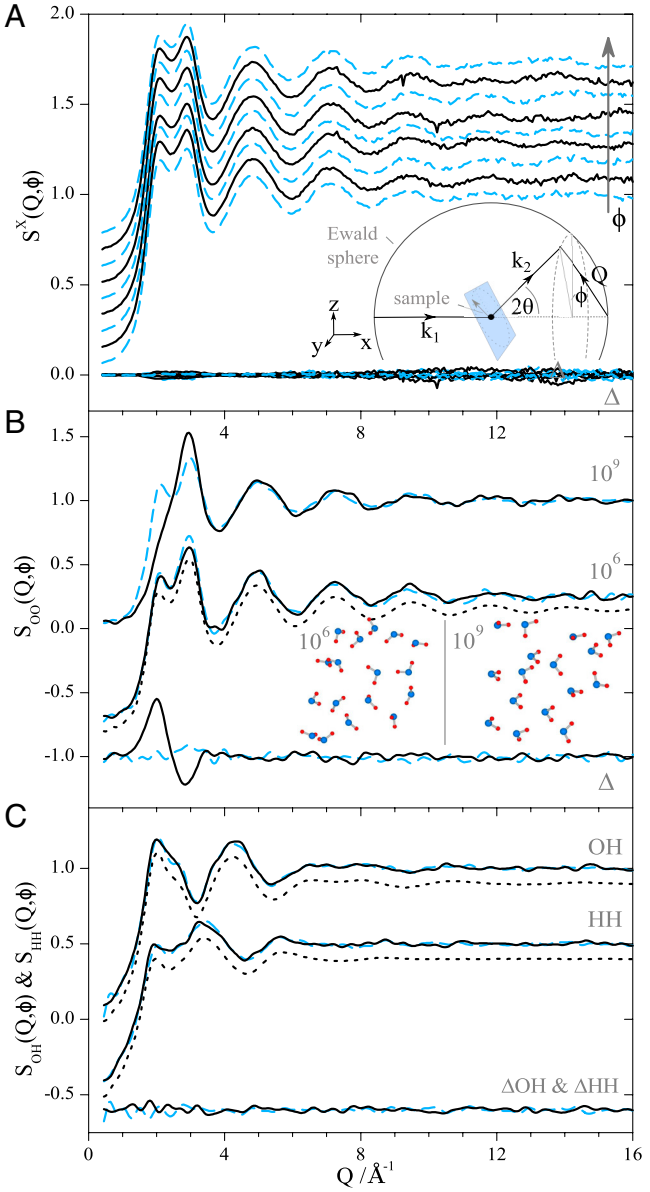

Fig. 4. (*A*) The upper curves are the directional $S^X(Q, \phi)$ diffraction patterns, from ϕ-slices of the diffraction image 10 degrees wide. The vertical gray arrow indicates the direction of increasing ϕ, from $\phi = 0$ (vertical, perpendicular to the E-field) to $\phi = 90$ (horizontal, along the E-field). The sample was a 26 °C, 7 mm long water bridge at 15.5 kV. The lower lines, labeled Δ are the slice minus average differences. These are within the measurement error. The *inset* shows a scattering diagram highlighting the direction of the **Q** vector, which rotates with both θ and ϕ. (*B*) Directional $S_{OO}(Q, \phi)$ patterns calculated from a TIP4P/2005 MD model, averaged over 400 time steps. The upper lines are from the 10^9 V/m model (density 0.0342 Å^{-3}). The blue dashed line corresponds to $\phi =$, (vertical) and black, $\phi = 90$ (horizontal). The middle lines are the same two ϕ-directions for the 10^6 V/m model (density 0.0335 Å^{-3}). The lower curves are the horizontal-vertical differences, for the 10^6 V/m (blue dashed line) and 10^9 V/m (black line) field strengths. *Inset* are 10 × 10 × 4 Å slices of the 10^6 V/m (left), and 10^9 V/m (right) models. (*C*) $\phi = 0$ (blue dashed lines) and $\phi = 90$ (black lines) OH and HH partial structure factors of the MD model at 10^6 V/m. The lower lines are the OH (blue dashed line) and HH (black line) horizontal-vertical differences. The gray dotted lines are the corresponding OO, OH, and HH structure factors of the MD model at 0 V/m. No significant difference is observed between the $\phi = 0$, and 90 directions at the 10^6 V/m field strength in either the MD model or the experimental data.

structures TIP4P/2005 Molecular Dynamics (MD) simulations were run, with external E-fields of 10^6 V/m and 10^9 V/m (see *Materials and Methods* for simulation details). This fixed

charge, pair potential simulation is not intended to exactly reproduce the water structure within the bridge, instead the 10^9 V/m field strength was chosen to provide a benchmark aligned structure. Whereas the 10^6 V/m field strength simulation contained very little molecular alignment, and is expected to be more representative of the E-field in the floating water bridge. In order to calculate the simulated structure factors of the anisotropic liquid from these MD simulations we have to go beyond the spherical Bessel function approximation of Debye (23) [2]. Instead the structure factors of the MD simulations were calculated retaining the directions of the scattering vector $\mathbf{Q}$ and pair separations $\mathbf{r}_{\alpha\beta}$ i.e.,

$$S_{ab}(\mathbf{Q}) - 1 = \frac{N}{N_a N_b}\left\langle \sum_{\alpha}^{N_a}\sum_{\beta\neq\alpha}^{N_b} \exp(i\mathbf{Q}\cdot\mathbf{r}_{\alpha\beta})\right\rangle \qquad [1]$$

$$\neq \frac{N}{N_a N_b}\left\langle \sum_{\alpha}^{N_a}\sum_{\beta\neq\alpha}^{N_b} \sin(Qr_{\alpha\beta})/(Qr_{\alpha\beta})\right\rangle. \qquad [2]$$

Where $S_{ab}(\mathbf{Q})$, is the pairwise partial structure factor for chemical species a and b. N is the total number of atoms in the simulation box. N_a is the number of atoms of chemical species a. The summations are over all distinct pair combinations α, β in the simulation box, and the brackets $\langle\rangle$ denote that the thermal average is taken. The dot product is calculated using the fact that the magnitude of $|\mathbf{Q}| = Q = 4\pi\sin(\theta)/\lambda$, and is given from geometry by

$$\mathbf{Q}\cdot\mathbf{r} = -Q\sin(\theta)r_x + Q\cos(\theta)\sin(\phi)r_y + Q\cos(\theta)\cos(\phi)r_z. \qquad [3]$$

Where ϕ is the angle of the Q-vector from the vertical z-axis, and 2θ is the scattering angle from the x-direction of the incident beam (see Fig. 4*A*, *Inset*). This dot product method makes no assumptions about symmetries in the sample (see *SI Text* for derivation). In principle the directional structure factor of any arrangement of atoms can be reconstructed this way, without the need for small angle, isotropic, nor Bragg approximations. For these reasons it is preferred to other methods such as expanding the Bessel function approximation to higher orders (for example see refs. 24 and 25), which usually retain some symmetry assumptions. This calculation is also useful for this work as it directly provides the structure factors in the same Q-space form as diffraction measurements.

The results of the directional structure factor analysis are plotted in Fig. 4*B*, which shows the oxygen-oxygen structure factors $S_{\mathrm{OO}}(Q,\phi)$, for ϕ parallel and perpendicular to the applied electric field in the MD models. Because it contributes over 90% of the signal in the X-ray measurements, $S_{\mathrm{OO}}(Q,\phi)$ was calculated at both 10^6 and 10^9 V/m field strengths. The large ϕ dependence of the directional $S_{\mathrm{OO}}(Q,\phi)$ patterns in the 10^9 V/m MD model confirms the sensitivity of the $S_{\mathrm{OO}}(Q,\phi)$ and hence $S^{\mathrm{X}}(Q,\phi)$ to molecular alignment. The large ϕ dependence of the 10^9 V/m model is in contrast to the measured $S^{\mathrm{X}}(Q,\phi)$, which was found to remain constant to within 2%, across all ϕ angles in the water bridge (Fig. 4*A*). The measured horizontal minus vertical differences in the water bridge were also essentially featureless in real space [Fig. 3, curve (D)]. For completeness the $S_{\mathrm{OH}}(Q,\phi)$ and $S_{\mathrm{HH}}(Q,\phi)$ of the 10^6 V/m MD model, are plotted in Fig. 4*C*. These oxygen-hydrogen (OH) and hydrogen-hydrogen (HH) partial structure factors contribute very little to the X-ray signal, but dominate neutron scattering patterns, and are expected to be more sensitive to molecular alignment than the OO distribution. Fig. 4*C* however, shows that like OO, the OH and HH structure factors at 10^6 V/m are isotropic, and equal to those of ambient water.

The similarity of the bridge water structure to ambient liquid water, and the lack of anisotropy, means that our results do not support the formation of any significant fraction of linear, chain-like structures within the bulk of the water bridge. This lack of anisotropy is also supported by previous theoretical studies where higher field strengths were required for alignment (26–29). The question therefore remains; how does the bridge form: If it is not a bulk structure effect, the answer probably lies in surface effects.

The effect of electric fields on the surface tension of water has been notoriously difficult to study and the results have been inconclusive with no general agreement (30–32). However, Bateni et al. have recently pioneered a new methodology to measure the surface tension of sessile droplets in electric fields (33, 34). They find that electric field strengths approximately 10^6 V/m increase the surface tension approximately 6%. This, and our bulk structure findings, support the conclusions of ref. 20 that relatively normal surface tensions are sufficient to provide the mechanical tension required. For example a 1 mm radius cylinder of water weighs approximately 3×10^{-4} N per centimeter of length, whereas the surface tension of ambient water is approximately 7×10^{-4} N/cm. Bateni et al. have also observed that the shape of water droplets changes significantly when a 5 kV electric potential is applied, acting against gravity (33, 34). This is in line with the electric field acting only on the surface to stabilize the shape of the water bridge, rather than affecting the bulk.

In conclusion we find the bulk structure of water within the floating water bridge to be isotropic, and the same as ordinary water at the same temperature. TIP4P/2005 MD calculations, at approximately the same field strength support this conclusion. The directional structure factor formalism given here is general, and does not require any symmetry assumptions of the sample. The lack of assumptions means that in principle any measured structure factor in a given ϕ-direction of any class of material can be directly compared to atomistic models. This method provides significantly more structural information, and a more stringent comparison to models, than traditional spherically averaged total scattering measurements. Some examples where this directional structure factor analysis may provide useful insight in future are amorphous and/or poorly crystalline fibers, liquid crystals, and disordered crystals.

Materials and Methods

The floating water bridge apparatus consisted of two 250 mL beakers, filled to within 5 mm of the top with 18 MΩ cm deionized water. One beaker was mounted on a translational stage, and the other was fixed. The beakers were placed so that the pouring lips were aligned, and platinum wire electrodes were placed in each beaker. A dc voltage, typically between 11 and 18 kV was applied to one electrode using a Trek P0621P, which was current limited to 0.5 mA. After a brief initial arcing, the water flowed up the beaker walls to connect and form a bridge. The movable beaker was slowly translated away from the other to extend the bridge length to between 5 mm and 25 mm. The surface temperature of the bridge was measured using two infrared thermal imaging cameras (Inframetrics model 760 and FLIR SC8000 series). The model 760 operated in the 8–12 micron range where the emissivity of water is known to be 0.96. The FLIR operated in the 3–5 micron range, and agreed with the model 760 measurement to within 2 °C implying an effective emissivity $\gtrsim$0.9 for the 3–5 micron range used by the FLIR. The bridges were formed repeatedly over several days and typically remained stable for 30 min or more.

An incident X-ray beam with an asymmetric 0.2 mm (vertical) × 0.5 mm (horizontal) rectangular cross-section was used. The Perkin Elmer XRD1621 flat plate area detector was off-centered 20 mm to avoid residual image effects from previous measurements, and placed 425–435 mm behind the sample. This setup provided a usable Q-range of 0.4–24 Å^{-1}, from the beam-stop to the nearest detector edge. The 760 infrared camera was aligned to be coincident with the X-ray beam, whereas the FLIR infrared camera gave a simultaneous temperature measurement of the entire water bridge during the experiment (see Fig. 1). The water bridge was precisely aligned to the X-ray beam by measuring the X-ray transmission with a photodiode detector. This transmission measurement also provided the dimensions of the water bridges formed, which varied between 7–11 mm in length, and

0.8–1.3 mm in diameter. The sample-detector distance was determined using a CeO_2 filled, thin-walled polyimide capillary, which was placed across the beakers where the water bridge formed. Placement of the calibrant relative to the water bridge was confirmed to within 0.2 mm using a surveyors leveling scope. The X-ray scattering data were analyzed and the X-ray structure factors extracted using standard methods applied to large area detectors as described in refs. 21 and 35. The ambient liquid water data shown in Fig. 2 was measured separately from a vertically downward flowing stream of water approximately 3 mm wide, at the same X-ray beamline (details to be published elsewhere).

In this work, the $S^X(Q)$ patterns have had the intramolecular OH and HH contributions subtracted through use of the molecular form factor calculated in ref. 36. The $S^X(Q)$ patterns were weighted using the commonly used $w^X = [\sum_a c_a f_a]^2$, where c_a and f_a are the concentration, and form factors of element species a. This weighting function has the advantage that the total weighting in $S^X(Q) \cong 1$ for all Q-values. The form factors used to calculate the w^X weighting function were taken from ref. 37 and modified to account for charge redistribution from H toward O, using the formula suggested by refs. 38 and 39. The X-ray distribution function $D^X(r)$, is then obtained from the measured $S^X(Q)$ by sine Fourier transformation as follows.

$$D^X(r) = 2/\pi \int_{Q_1}^{Q_2} Q[S^X(Q) - 1] \sin(Qr) dQ. \qquad [4]$$

Where Q_1 and Q_2 are the minimum and maximum measured Q-values (see refs. 35 and 40 for further detail and definitions). The higher number of electrons on oxygen vs. hydrogen, coupled with the redistribution of charge toward the oxygen in the O—H bond, results in an oxygen-oxygen weighting that varies from approximately 80% at $Q = 0$, to ≥95% at $Q \geq 12$ Å^{-1}, in the X-ray measurements. This strong OO weighting is why the X-ray measurement essentially describes the distribution of molecule centers, with only a minor intermolecular OH contribution and negligible intermolecular HH contribution.

The MD structure in Fig. 4 was generated from a TIP4P/2005 (41) simulation on 1,000 water molecules, implemented within the DL_POLY classic MD package (42). The TIP4P/2005 potential was chosen because it reproduces ambient liquid water structure more accurately than other empirical potential models (43). First principles, or DFT models were not considered, as the size of this simulation was required to be $\gtrsim$1,000 molecules to reproduce the experimentally observed Q and r ranges. The E-fields used in this fixed charge model were 10^6 and 10^9 V/m. The 10^9 V/m field strength simulation was not intended to reproduce the bridge structure, but was chosen to demonstrate the sensitivity of the directional structure factor technique to aligned water structures. To compare to the measured $S^X(Q, \phi)$, where ϕ was averaged over slices 10 degrees wide, the simulated $S_{OO}(Q, \phi)$, were also averaged from several ϕ points over the same range. Also, to reduce noise in both the simulation and measurements, 180 degree opposing ϕ-directions were averaged together. Because the MD model only calculates a full sphere of atom separations up to half the box side length (r_m), larger separations were neglected. This results in an $S(Q)$ which transforms to give a pair distribution function which is truncated to zero for $r \geq r_m$. To correct for the truncation we added the function $C(Q)$ to the $S(Q)$ calculated using [2] where

$$C(Q) = \frac{4\pi\rho(Q\cos(Qr_m) - \sin(Qr_m)).}{Q^3} \qquad [5]$$

This $C(Q)$ is taken from ref. 45, and was chosen because its real space Fourier transform is a step function which =0 at and below r_m and =1 above r_m. Use of this $C(Q)$ function essentially substitutes the missing higher-r structural information, with the macroscopic density of the material; i.e., the assumption $g(r) = 1$ (or $D(r) = 0$), for $r \geq r_m$ is made. For the 1,000 molecule simulations performed in this work the $r_m \approx 15.5$ Å, where the distribution functions are already very close to the assumed macroscopic limit.

ACKNOWLEDGMENTS. Our thanks to Jeff Collins, Rick Spence, Sonia Tumber, William Woerner, and Bruce Glagola for their technical expertise. Also thanks to Adrian Barnes for useful discussion. We acknowledge support from contract number DE-FG02-09ER46650 for funding of L.B.S. and J.B.P., including data collection and analysis and the production of this manuscript. This work was also supported by the DOE at the Advanced Photon Source (Argonne, Il, USA), under contract number DE-AC02-06CH11357. B.S. was supported by grant number DE-FC52-08NA28554.

1. Vemulapalli GK, Kukolich SG (1996) Why does a stream of water deflect in an electric field? *J Chem Educ* 73:887–888.
2. Bramwell ST (1999) Condensed-matter science: Ferroelectric ice. *Nature* 397:212–213.
3. Toney MF, et al. (1994) Voltage-dependent ordering of water molecules at an electrode-deelectrolyte interface. *Nature* 368:444–446.
4. Stumm W (1997) Reactivity at the mineral-water interface: Dissolution and inhibition. *Colloid Surface A* 120:143–166.
5. Honig B, Nicholls A (1995) Classical electrostatics in biology and chemistry. *Science* 268:1144–1149.
6. Fuchs EC, et al. (2007) The floating water bridge. *J Phys D Appl Phys* 40:6112.
7. Taylor G (1964) Disintegration of water drops in an electric field. *Proc R Soc Lond A* 280:383–397.
8. Fuchs EC, et al. (2009) Neutron scattering of a floating heavy water bridge. *J Phys D Appl Phys* 42:065502.
9. Fuchs EC, et al. (2010) Two-dimensional neutron scattering in a floating heavy water bridge. *J Phys D Appl Phys* 43:105502.
10. Rai D, Kulkarni AD, Gejji SP, Pathak RK (2008) Water clusters $(H_2O)n$ $n = 6$–8, in external electric fields. *J Chem Phys* 128:034310.
11. Fuchs EC, Gatterer K, Holler G, Woisetschläger J (2008) Dynamics of the floating water bridge. *J Phys D Appl Phys* 41:185502.
12. Woisetschläger J, et al. (2010) Horizontal bridges in polar dielectric liquids. *Exp Fluid* 52:193–205.
13. Piatkowski L, et al. (2012) Ultrafast vibrational energy relaxation of the water bridge. *Phys Chem Chem Phys* 14:6160–6164.
14. Hand E (2007) Water doesn't mind the gap. *Nature* 449:517.
15. Wei S, Xiaobin X, Hong Z, Chuanxiang X (2008) Effects of dipole polarization of water molecules on ice formation under an electrostatic field. *Cryobiology* 56:93–99.
16. Hülsheger H, Potel J, Niemann E-G (1983) Electric field effects on bacteria and yeast cells. *Radiat Environ Biophys* 22:149–162.
17. Ponterio RC, et al. (2010) Raman scattering measurements on a floating water bridge. *J Phys D Appl Phys* 43:175405.
18. Vegiri RC, et al. (2004) Origin of the enhanced structural and reorientational relaxation rates in the presence of relatively weak dc electric fields. *Pure Appl Chem* 76:215–221.
19. Cramer T, Zerbetto F, Garcia R (2008) Molecular mechanism of water bridge buildup: Field-induced formation of nanoscale Menisci. *Langmuir* 24:6116–6120.
20. Aerov AA (2011) Why the water bridge does not collapse. *Phys Rev E* 84:036314.
21. Skinner LB, Benmore CJ, Parise JB (2012) Area detector corrections for high quality synchrotron X-ray structure factor measurements. *Nucl Instrum Methods A* 662:61–70.
22. Narten AH, Levy HA (1971) Liquid water: Molecular correlation functions from X-ray diffraction. *J Chem Phys* 5:2263–269.
23. Debye P (1915) Zerstreuung von Röntgenstrahlen. *Ann Phys* 46:809–823.
24. Suzuki Y, Haimovich J, Egami T (1987) Bond-orientational anisotropy in metallic glasses observed by X-ray diffraction. *Phys Rev B* 35:2162–2168.
25. Vempati UK, Valavala PK, Falk ML, Almer J, Hufnagel TC (2012) Length-scale dependence of elastic strain from scattering measurements in metallic glasses. *Phys Rev B* 85:214201.
26. Acosta-Gutierrez S, Hernandez-Rojas J, Breton J, Gomez Llorente JM, Wales DJ (2011) Physical properties of small water clusters in low and moderate electric fields. *J Chem Phys* 135:124303.
27. Hernandez-Rojas J, Gonzalez BS, James T, Wales DJ (2006) Thermodynamics of water octamer in a uniform electric field. *J Chem Phys* 125:224302.
28. James T, Wales DJ, Hernandez-Rojas J (2007) Energy landscapes for water clusters in a uniform electric field. *J Chem Phys* 126:054506.
29. Jung DH, Yang JH, Jhon MS (1999) The effect of an external electric field on the structure of liquid water using molecular dynamics simulations. *Chem Phys* 244:331–337.
30. Hayes CF (1975) Water-air interface in the presence of an applied electric field. *J Phys Chem* 79:1689–1693.
31. Liggieri L, Sanfeild A, Steinchen A (1994) Effects of magnetic and electric fields on surface tension of liquids. *Phys A Stat Mech Appl* 206:299–331.
32. Goodismann J (1992) Surface tension of a charged and polarized system. *J Phys Chem* 96:6355–6360.
33. Bateni A, Amirfazli A, Neumann AW (2006) Effects of an electric field on the surface tension of conducting drops. *Colloid Surface A* 289:25–38.
34. Bateni A, Susnar SS, Amirfazli A, Neumann AW (2004) Development of a new methodology to study drop shape and surface tension in electric fields. *Langmuir* 20:7589–7597.
35. Fischer HE, Barnes AC, Salmon PS (2006) Neutron and X-ray diffraction studies of liquids and glasses. *Rep Prog Phys* 69:233–299.
36. Wang J, Tripathi AN, Smith VH (1994) Chemical binding and electron correlation effects in X-ray and high energy electron scattering. *J Chem Phys* 101:4842–4854.
37. Hubbell JH, Øverbro I (1979) Relativistic atomic form factors and photon coherent scattering cross sections. *J Phys Chem Ref Data* 8:69–105.
38. Soper AK (2007) Joint structure refinement of X-ray and neutron diffraction data on disordered materials: Application to liquid water. *J Phys Condens Matt* 19:335206.
39. Sorenson JM, Hura G, Glaeser RM, Head-Gordon T (2000) What can X-ray scattering tell us about the radial distribution functions of water? *J Chem Phys* 113:9149–9161.

40. Keen DA (2000) A comparison of various commonly used correlation functions for describing total scattering. *J Appl Crystallogr* 34:172–177.
41. Abascal JLF, Vega C (2005) A general purpose model for the condensed phases of water: TIP4P/2005. *J Chem Phys* 123:234505.
42. Smith W, Forester TR (1996) DL_POLY 2. 0a general-purpose parallel molecular dynamics package. *J Mol Graph* 14:136–141.
43. Neuefeind J, Benmore CJ, Weber JKR, Pashek D (2011) More accurate X-ray scattering data of deeply supercooled bulk liquid water. *Mol Phys* 109:279–288.
44. Lorch E (1969) Neutron diffraction by germania, silica and radiation-damaged silica glasses. *Phys C Solid State Phys* 2:229–237.
45. Narten AH (1972) Diffraction pattern and structure of noncrystalline BeF_2 and SiO_2 at 25 °C. *J Chem Phys* 56:1905–1909.